JGR Space Physics

RESEARCH ARTICLE
10.1029/2018JA025582

Global Energy Dynamics During Substorms on 9 March 2008 and 26 February 2008 Using Satellite Observations and the WINDMI Model

E. Spencer[1], P. Srinivas[1], and S. K. Vadepu[1]

[1]Electrical and Computer Engineering Department, University of South Alabama, Mobile, AL, USA

Key Points:
- Substorms can be captured by the low-order WINDMI nonlinear physics-based model over a large dynamic range of solar wind conditions
- Two vastly different substorms in terms of solar wind forcing (40 kV vs. 300 kV) are captured using only four variable parameters
- Model onsets were about 5 to 10 min earlier than the reported onsets; timing depends strongly on solar wind propagation from L1

Correspondence to:
E. Spencer,
espencer@southalabama.edu

Citation:
Spencer, E. A., Srinivas, P., & Vadepu, S. K. (2019). Global energy dynamics during substorms on 9 March 2008 and 26 February 2008 using satellite observations and the WINDMI model. *Journal of Geophysical Research: Space Physics, 124*, 1698–1710. https://doi.org/10.1029/2018JA025582

Received 12 APR 2018
Accepted 23 FEB 2019
Accepted article online 7 MAR 2019
Published online 22 MAR 2019

Abstract We analyze three substorms that occur on (1) 9 March 2008 05:14 UT, (2) 26 February 2008 04:05 UT, and (3) 26 February 2008 04:55 UT. Using ACE solar wind velocity and interplanetary magnetic field B_z values, we calculate the rectified (southward B_z) solar wind voltage propagated to the magnetosphere. The solar wind conditions for the two events were vastly different, 300 kV for 9 March 2008 substorm, compared to 50 kV for 26 February 2008. The voltage is input to a nonlinear physics-based model of the magnetosphere called WINDMI. The output is the westward auroral electrojet current which is proportional to the auroral electrojet (AL) index from World Data Center for Geomagnetism Kyoto and the SuperMAG auroral electrojet index (SML). Substorm onset times are obtained from the superMAG substorm database, Pu et al. (2010, https://doi.org/10.1029/2009JA014217), Lui (2011, https://doi.org/10.1029/2010JA016078) and synchronized to Time History of Events and Macroscale Interactions during Substorms satellite data. The timing of onset, model parameters, and intermediate state space variables are analyzed. The model onsets occurred about 5 to 10 min earlier than the reported onsets. Onsets occurred when the geotail current in the WINDMI model reached a critical threshold of 6.2 MA for the 9 March 2008 event, while, in contrast, a critical threshold of 2.1 MA was obtained for the two 26 February 2008 events. The model estimates 1.99 PJ of total energy transfer during the 9 March 2008 event, with 0.95 PJ deposited in the ionosphere. The smaller events on 26 February 2008 resulted in a total energy transfer of 0.37 PJ according to the model, with 0.095 PJ deposited in the ionosphere.

Plain Language Summary A low-dimensional model of the magnetosphere called WINDMI is used to analyze the energy flow and dynamics during substorms. The model is used to predict ground-based magnetic indices that are related to geomagnetic activity driven by the solar wind.

1. Introduction

During substorm activity, it is of interest to quantify the electromagnetic energy components and plasma conditions in the Earth's magnetotail in order to understand how the dynamics evolve. Under different solar wind velocity and interplanetary magnetic field forcing, the magnetosphere is configured into distinct physical states that trigger substorms for different combinations of geotail current, plasma sheet pressure, $\vec{E} \times \vec{B}$ flow, and ionospheric variables.

Substorm onset is preceded by a growth phase (McPherron, 1970), when the magnetic energy in the geotail gradually increases, which further stretches the magnetotail (Meurant et al., 2007). At some critical threshold, onset occurs, and the energy is released, resulting in a reconfiguration of the magnetotail (Baker et al., 1999). Finally, the magnetotail settles back into the pregrowth stretched configuration during the recovery phase. Depending on solar wind and plasma conditions, several onset and recovery phases may occur before the overall activity concludes (Partamies et al., 2013).

Investigating the flow of energy between different components of the nightside magnetosphere is important, because they control the rates and amplitudes of the growth, onset, expansion, and recovery phases. In an early study, Baker et al. (1985) examined the role of magnetotail storage and rapid dissipation of energy during substorms. Tanskanen et al. (2002a) compared substorm energy budgets during low and high solar activity. Akasofu (2013) discuss the accumulation of magnetic energy in the geotail prior to the expansion phase. Miyashita et al. (2004) used 397 substorms to study the difference between intense and weak substorms, in terms of onset location, pressure, and Poynting flux.

The primary source of energy that drives geomagnetic activity is the solar wind. Newell et al. (2007), Akasofu (1981), and others give so-called solar wind coupling functions that provide the energy input into the magnetosphere as a function of the solar wind velocity, interplanetary magnetic field (IMF) values, IMF orientation, and in some cases, the solar wind dynamic pressure. Some of these coupling functions have been previously evaluated with the WINDMI model by Spencer et al. (2009, 2011). These solar wind parameters are measured at the ACE satellite, located at the L1 Lagrangian point, at about 250 Earth radii from the Earth, toward the Sun. The solar wind parameters are propagated to the nose of the Earth's magnetosphere, using various techniques including taking into account the IMF phase plane, under the assumption that the solar wind structure does not alter significantly in transit (Weimer & King, 2008). A time uncertainty of ±10 min for the propagation delay is expected (Mailyan et al., 2008).

From a dynamical perspective, the energy flow from the solar wind through the magnetosphere is characterized by time constants that in principle may be estimated through a circuit-like approach (Horton & Doxas, 1996, 1998; Nakai & Kamide, 2005; Ohtani & Uozumi, 2014). These time constants, geotail lobe inductance, plasma sheet capacitance, conductances, and plasma loss rates, could be used to constrain higher-order models such as global MHD simulations. The associated energy variables, such as the geotail magnetic field, plasma flow velocities, cross-tail electric field, field-aligned currents, ionosphere electric fields, and electrojet currents are then restricted in their time rates of change as well as their values when critical changes occur, such as substorm onset (Huang & Cai, 2009).

In order to accurately quantify the energy flow between the geotail, plasma sheet and field-aligned currents, coordinated measurements of substorm events are necessary. Identifying the different phases of a substorm from either the Kyoto World Data Center AE and AL indices or the SuperMAG SML index can be challenging (Forsyth et al., 2015), while satellite measurements depend on fortuitous conjunctions (Lui, 2011). To circumvent this, Kallio et al. (2000) examined loading-unloading processes during magnetospheric substorms with the IL index, a local, midnight sector version of the AL index from the IMAGE magnetometer chain together with solar wind and IMF data from the WIND spacecraft.

Some electrojet activity are associated with pseudobreakups (Kullen et al., 2010), posing additional difficulties in the discrimination between phases.

In this paper, we analyze three substorms that occur on the following dates: (1) 9 March 2008 05:14 UT, (2) 26 February 2008 04:00 UT, and (3) 26 February 2008 04:55 UT with the WINDMI model. The WINDMI model is a physics-based, nonlinear model of the nightside magnetosphere. It uses the solar wind velocity and magnetic fields as input and produces the region 1 field-aligned current that closes in the ionosphere as the westward auroral electrojet as output. The output is compared to the Kyoto AL index and the SuperMAG SML indices. We are interested in the global energy flows and the overall dynamical behavior of the magnetosphere during substorms. We also want to establish the minimum required variables in the WINDMI model in order to reliably capture substorms of different strengths.

On 9 March 2008, the aurora was more active than during typical isolated substorms because it was a storm time event. There were several arcs that were observed starting from 0513 UT to 0541 UT including a pseudo breakup at 0529 UT (Xing et al., 2010). The superMAG database reports a substorm onset at 05:14 UT. On 26 February 2008, the THEMIS spacecraft observed two distinct substorms expansion onsets that were triggered 50 min apart. These events were studied in depth with regard to possible onset mechanisms by Pu et al. (2010) and Lui (2011).

In this work we use the solar wind velocity and IMF data on 9 March 2008 and 26 February 2008 to drive a low-order nonlinear physics-based WINDMI model of the nightside magnetosphere. The model outputs are compared to the auroral AL and SML indices obtained from World Data Center Kyoto and SuperMAG facilities, respectively. We place constraints on the WINDMI model so that the observed signatures and measurements coincide as closely as possible with the model state variables. THEMIS measurements of ion velocity, electric fields, and magnetic fields are used to establish the time sequence of the onset, expansion, and recovery phases. We allow only four parameters to be adjustable. These parameters control the substorm trigger mechanism in the WINDMI model and level of ionosphere activity, as we will briefly describe below.

In section 2, we summarize the substorm event data, drawing from the references. In section 3, we present our model results, and how they were obtained. In section 4, we discuss our interpretation of the model results and finally draw some conclusions in section 5.

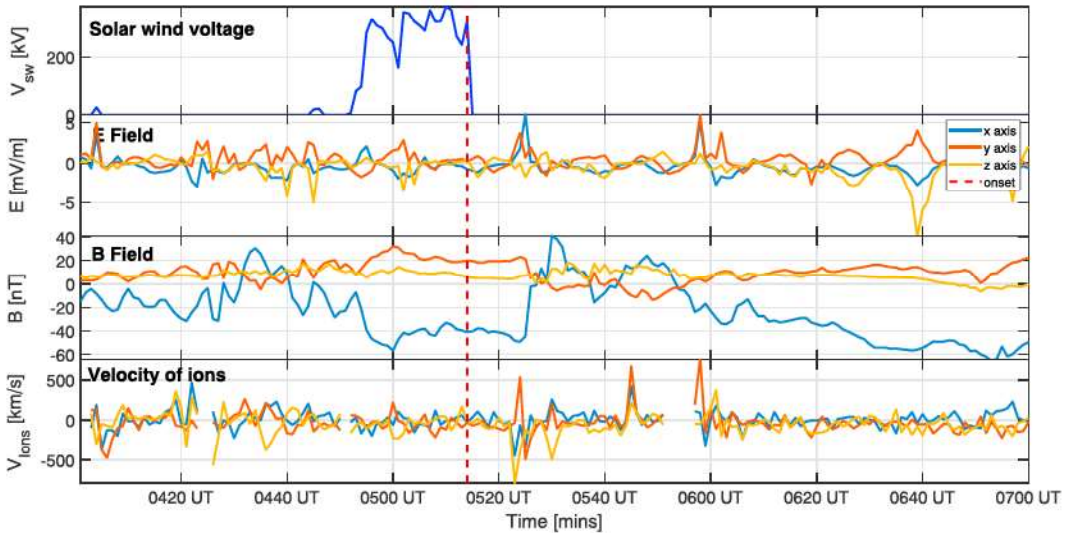

Figure 1. From top to bottom, the first panel shows solar wind input (rectified *VBs*) calculated from ACE measurements. The second and fourth panels show *E* field and Ion velocity from THEMIS B. The third panel shows *B* field from THEMIS D. Onset is marked with vertical line at 05:14 UT.

2. Substorm Data

Solar wind velocity and IMF B_z are obtained from the ACE satellite data repository at the NASA Space Physics Data Facility. We propagate the solar wind parameters from L1 to the nose of the magnetosphere assuming pure convection. For the 9 March 2008 event, we propagated it by 49 min, while for the 26 February events, we propagated it by 70 min. The propagation time is obtained by dividing 250 R_E by the average *x*-directed velocity of the solar wind over a 2-hr interval including the event interval.

In order to determine the substorm onset time, Time History of Events and Macroscale Interactions during Substorms (THEMIS) electric, magnetic and ion velocity data were obtained via the Berkeley THEMIS website. The westward auroral electrojet strength is obtained from the Kyoto World Data Center AL index. This is additionally compared to the SuperMAG SML index, which is an alternate measure of the westward auroral electrojet strength.

In order to drive the WINDMI model, we calculate an effective rectified (southward IMF B_z is active) voltage using the ACE solar wind *x*-directed velocity, IMF B_z values and an effective width of the dayside magnetosphere reconnection line. This is given by

$$V_{\mathrm{sw}}^{\mathrm{Bs}} = V_0 + v_{\mathrm{sw}} B_s^{\mathrm{IMF}} L_y^{\mathrm{eff}} \tag{1}$$

when $B_z < 0$. Here $V_0 = 4$ kV is a base viscous driving voltage, and $L_y = 10R_e$. Although other coupling functions are available, the rectified *VBs* voltage, as given above, was chosen because it provides a clear and unbiased starting point to discussing how the growth, onset, expansion, and recovery phases are related to the global energy storage and dynamics. Usually, a base viscous (during northward IMF B_z) voltage is applied to the model to generate the DC offset required to match the AL during the *VBs* inactive period, but here we purposely applied a very low (4-kV) base voltage to emphasize the substorm timing.

2.1. The 9 March 2008 at 05:14 UT Event

During this event, the THEMIS spacecraft was located close to the center of the plasma sheet. The onset time was determined by the THEMIS all-sky imager SNKQ FOV (Xing et al., 2010). The all-sky imagers indicated that brightening lasted from 05:24:00 to 05:42:00 UT with four major intensifications.

According to (Xing et al., 2010), a substorm is initiated at 05:41 UT. However, the AL and SML do not show any strong activity at that time, which precludes our being able to use it. The IMF B_z is southward roughly between 04:45 UT and 05:15 UT. Hence, the derived rectified *VBs* voltage input that is needed for the WINDMI model is only active during this period. This can be seen in the first panel of Figure 1. Beyond 05:15 UT there is no solar wind driving available for the WINDMI model. The superMAG substorm identification algorithm (Newell & Gjerloev, 2011a, 2011b), which contains more than 53,000 substorms from 1

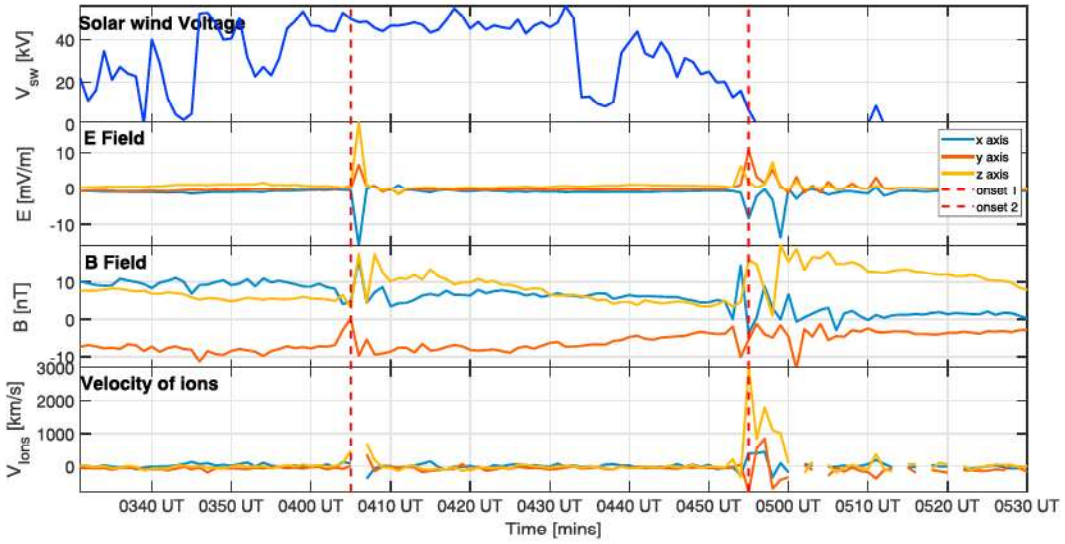

Figure 2. From top to bottom, the first panel shows solar wind input (rectified *VBs*) calculated from ACE measurements. The second and fourth panels show *E* field and ion velocity from THEMIS E. Onsets are at 04:05 UT and 04:55 UT.

January 1980 to 31 December 2009, reports a substorm initiation at 05:14 UT, and this is coincident with the AL and SML signatures. The peak SML and AL occurs at 05:24 UT, which corresponds to a burst of activity observed by the THEMIS B and D spacecraft. In Figure 1, there is a jump in B_x, and a rapid fluctuation in the electric field and ion velocity measurements around 05:24 UT. We chose to be consistent with the SML data set and the AL index and set the onset time of a substorm at 05:14 UT.

At 05:24 UT the THEMIS B and D spacecraft were located at $(-18, 5, 4)\ R_e$ and $(-10, 4, -3)\ R_e$ respectively. In Figure 1, the solar wind-derived input voltage and the THEMIS satellite measurements are shown. The solar wind input voltage reaches levels at around 300–350 kV for a period of 20–25 min before subsiding at onset. THEMIS B electric field and ion velocity measurements show surges of 5 mV/m and 400 km/s, respectively, at 05:24 UT. THEMIS D magnetic field B_x measurements (third panel of Figure 1) show what appears to be a dipolarization occurring at 05:24 UT. In the same plot we observe signatures of magnetotail stretching before 05:24 UT, and a slow recovery after the expansion phase, lasting to about 07:00 UT. First B_x becomes more negative, then turns positive abruptly, and returns back to negative.

2.2. The 26 February 2008 at 04:05 UT and 04:55 UT Events

On this date, two weak substorms occurred, one at 04:05 UT and another at 04:55 UT. For both events, the THEMIS satellites were close to the plasma sheet. The onset times are taken from Lui (2011) and Pu et al. (2010).

During the first event, data from SKNQ and GILL all-sky imagers indicate that there were two auroral intensifications, the second stronger intensification was at 04:04:30 UT nearer to the midnight sector. The THEMIS E spacecraft was located at $(-4.5, 5.2, -0.1)\ R_e$. During the second event, the first auroral intensification was noticed by GILL all-sky imager at 04:51:40 UT and the second auroral intensification was observed by SNKQ all-sky imager at 04:53:05 UT, and then the arc went on to expand and become brighter. The THEMIS E spacecraft was located at $(-4.5, 5.2, -0.1)\ R_e$.

In Figure 2, the onset times are shown together with the solar wind input voltage and THEMIS E measurements of electric fields, magnetic fields, and ion velocity. During this event, the input voltage is no more than about 50 kV and drops quickly prior to the second substorm sequence. Again, the IMF B_z turns northward at about the time the onset occurs, although this is subject to the uncertainty in the solar wind propagation time from L1.

3. Results

We set up the WINDMI model to be as similar as possible between the two events. The model parameters that involved ionosphere and ring current variables were held constant. However, to obtain our results, we

did allow the ionosphere conductivity Σ_I to be variable, in addition to the substorm trigger parameters, as will be discussed below.

Although we use the complete WINDMI model in our runs, the substorm trigger is in fact controlled by the first four equations of the model. For the purposes of analysis, we can neglect the mutual inductance M between the geotail current and the field-aligned current. The internal dynamics of the magnetosphere is then represented by

$$L\frac{dI}{dt} = V_{sw}(t) - V \tag{2}$$

$$C\frac{dV}{dt} = I - I_1 - I_{ps} - \Sigma V \tag{3}$$

$$\frac{3}{2}\frac{dp}{dt} = \frac{\Sigma V^2}{\Omega_{cps}} - u_0 p K_{\parallel}^{1/2}\Theta(u_1) - \frac{pVA_{eff}}{\Omega_{cps}B_{tr}L_y} - \frac{3p}{2\tau_E} \tag{4}$$

$$\frac{dK_{\parallel}}{dt} = I_{ps}V - \frac{K_{\parallel}}{\tau_{\parallel}} \tag{5}$$

where $\Theta(u_1) = 1/2[1 + \tanh[(I - I_c)/\Delta I]$.

Equation (2) describes the energy flow between the solar wind and the geotail current. Equation (3) is the rate of change of $\vec{E} \times \vec{B}$ flows due to forces in the plasma sheet. Equation (4) describes the thermal pressure in the plasma sheet and contains the substorm trigger. Equation (5) gives the parallel flow of kinetic energy along field lines. These are the first four of the eight equations in the complete WINDMI model. When the model is constrained in this manner, the energy flow and dissipation to the ring current is held constant. The ionosphere dynamics are also held constant, except that the auroral electrojet strength is controlled by Σ_I. Only the energy conversion between the solar wind and the plasma sheet, and the electrojet strength, is allowed to vary.

The parameters that strongly influence the initiation of a substorm are L the geotail inductance, C the plasma sheet capacitance, Σ the plasma sheet conductivity, and I_c the critical geotail current threshold for substorm triggering. Some other parameters are held constant at the following values, $\tau_E = 1$ hr, $A_{eff} = 2R_E^2$, $\Omega_{cps} = 4{,}000\ R_E^3$, $B_{tr} = 5$ nT, $u_0 = 4.2 \times 10^9$, and $\tau_{\parallel} = 10$ min. The remaining parameters are held constant at nominal values. Tables A1 and A2 in the appendix explain these parameters more completely and give their nominal values. Only four parameters, C, Σ, I_c, and Σ_I were optimized to match the model output to the AL and SML indices. In previous work all the parameters of the model (Spencer et al., 2007) were optimized against substorm data computationally. Here, we use manual optimization to extract more qualitative information.

In the WINDMI model the geotail energy content W_m is given by $W_m = 1/2LI^2$ where L is the geotail inductance and I is the geotail current. If we assume the magnetotail configuration is such that $Lx = 50\,R_e$, $Ly = 20\,R_e$, and $Lz = 20\,R_e$, we get a value of $L = 32$ H, assuming a solenoidal-like magnetotail. Nominally, we set the inductance of the geotail lobe at $L = 50$ H.

If $L = 50$ H and the geotail current I is about 5 MA, we have a stored energy value in the magnetotail of roughly 6.25×10^{14} Joules according to the model. This was the case on average for the level of activity on 9 March 2008. In contrast, the 26 February 2008 pair of events had roughly half of that energy level stored in the magnetotail according to the model. At 300 kV it takes roughly 14 min to energize the magnetotail to 5 MA, while at 50 kV it takes 42 min to reach 2.5 MA. These estimates are from assuming a ramp current build up across the geotail inductance with constant input voltage, $\Delta t = L\Delta I_{gt}/V$. Here Δt is the time period over which a change of geotail current ΔI_{gt} occurs. V is the applied constant voltage.

The global linear dynamics are represented by a parallel RLC circuit ($R = 1/\Sigma$), influenced by L, C, and Σ. The oscillation frequency is given by $\sqrt{1/LC - (\Sigma/2C)^2}$, and damped at a rate $\exp(-\Sigma t/2C)$. Using $L = 50$ H, $C = 5{,}000$ F, and $\Sigma = 10$, we get a global oscillation period of about 47 min, and a decay rate of about 17 min (The amplitude drops to e^{-1} of any original amplitude in 17 min). It may be possible to observe this damped oscillatory behavior when the solar wind driving amplitudes are low.

Although the geotail inductance L is a variable parameter, it represents the geometrical dimensions of the magnetotail, which should not be changing substantially. We therefore held it constant at 50 H. Only three

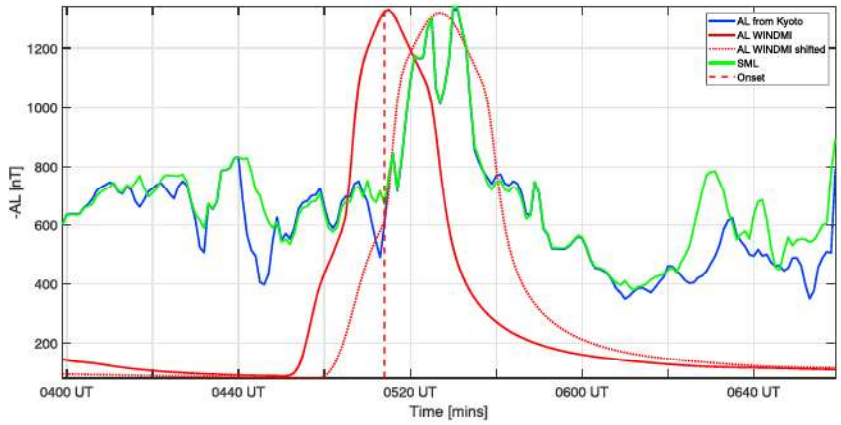

Figure 3. WINDMI model predictions compared to AL index (Kyoto World Data Center) and SML index (SuperMAG). Model onset is 9 min before reported onset. Model AL peak occurs 10 mins before actual AL and SML peak. The dotted red curve shows the effect of an additional time shift of 9 min applied to solar wind input.

parameters in the equations above were varied to obtain a triggering condition, while Σ_I in equation (A6) was varied to match the AL and SML indices in amplitude.

We allowed for the possibility of error in solar wind propagation times by shifting the input voltage in time forward or backward by no more than 10 mins if it improved our results. We show both the nominal and shifted results in our plots, and discuss the implications in section 4.

3.1. The 9 March 2008 Results

In Figure 3, the Kyoto AL index, SuperMAG SML index, and the WINDMI AL output, are shown. The substorm onset is marked by the red vertical dotted line at min 314 (05:14 UT). The AL maximum occurs at 05:24, but the WINDMI output peaks 9 min earlier. The substorm is initiated in the model for $C = 3{,}000$ F, $\Sigma = 8.8$ S, and $I_c = 6.2$ MA. The global oscillation period here is about 49 min. The ionosphere conductivity was high, $\Sigma_I = 24$ S according to the model. This was necessary for the model to produce the peak surge of about 1,400 nT observed in both the AL and SML indices. The model triggers at about 05:05 UT with the nominally applied time shift. However, if an additional shift of 9 min is added, based on onset matching, the model triggers at 05:14 UT. This is done with the parameters held fixed. Now the model peak corresponds well with the AL and SML indices. A second surge appears clearly in the SML index at 06:30 UT, but there is no solar wind driving voltage present for the model to produce any output.

In Figure 4, the top panel shows the model cross-tail electric field, and the bottom panel shows the model geotail current. The model gives a 2.5-mV/m peak electric field value, but the THEMIS measurement

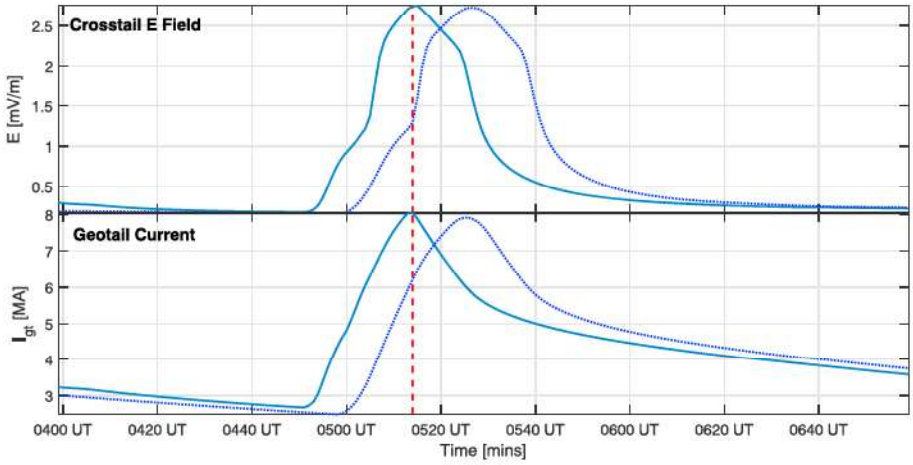

Figure 4. The large scale (top) cross-tail electric field and (bottom) geotail current obtained from the WINDMI model for 9 March 2008. Model parameters: $L = 50$ H, $Ic = 6.2$ MA, $C = 3{,}000$ F, $\Sigma = 8.8$ S, $\Omega_{\text{cps}} = 4{,}000\ R_E^3$.

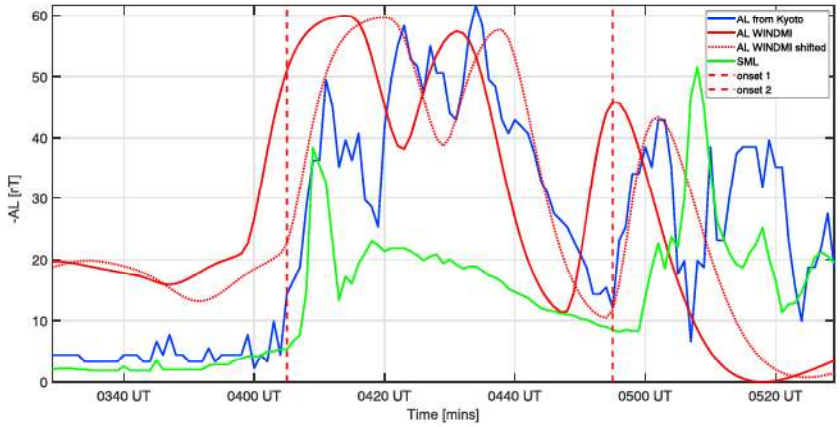

Figure 5. WINDMI model predictions compared to AL index (Kyoto World Data Center) and SML index (SuperMAG). Model onset occurs 5 min before the first reported onset and 7 min before the second reported onset. The dotted red curve shows the effect of an additional time shift of 5 min applied to solar wind input.

showed closer to 4 mV/m (E_y). This may be as a result of the simulated electric field being calculated from the model crosstail voltage divided by $L_y = 10R_e$.

We estimate the energy budget for this event using the electric field and geotail current plots in Figure 4. The energy flow $W = \int_T EL_y I dt$ is calculated from 04:50 UT to 06:00 UT. Here the time $T = 70$ min is the overall time interval of the substorm. The total energy flow over the substorm interval is 1.99 PJ according to the model. which is consistent with Tanskanen et al. (2002a). With our parameter uncertainties our energy estimates have about 10% uncertainty.

The proportion of this energy deposited into the ionosphere is obtained by performing a similar integral but now using the ionosphere voltage V_I in equation (A6) between the footpoints of the region 1 FAC together with $I1$ in equation (A5) (proportional to the westward auroral electrojet). The energy transferred to the ionosphere is 0.95 PJ, or roughly half the total energy transfer, in this case. This is consistent with the levels reported in Tanskanen et al. (2002b).

The plasma $E \times B$ drift velocity can be estimated using the electric field values obtained from the model and assuming a nominal B_z in the plasma sheet of 10 nT. The maximum $E \times B$ velocity using $E = 4$ mV/m and $B_z = 10$ nT is 400 km/s.

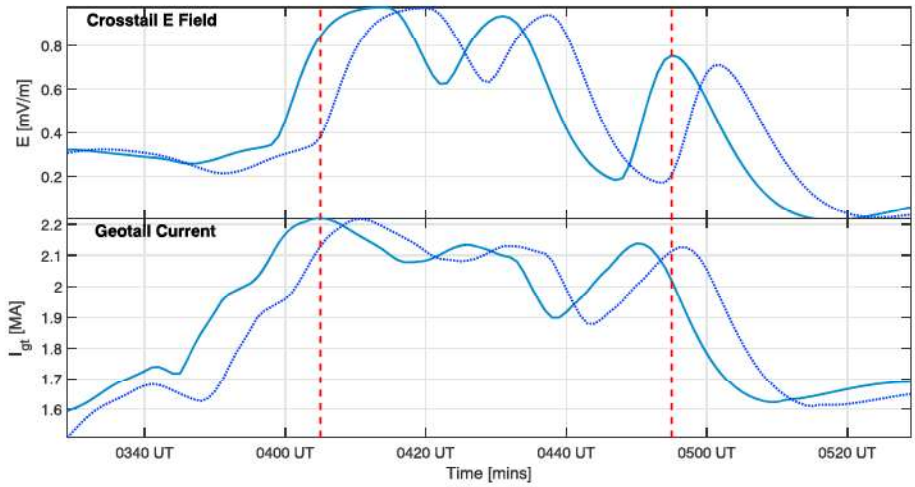

Figure 6. The large scale (top) cross-tail electric field and (bottom) geotail current obtained from the WINDMI model for 26 February 2008. Model parameters: $L = 50$ H, $Ic = 2.1$ MA, $C = 8{,}000$ F, $\Sigma = 8$ S, $\Omega_{\text{cps}} = 4{,}000\ R_E^3$.

Table 1
Significant Parameters and Features Calculated With the WINDMI Model for the Two Events Analyzed in This Paper

Event	Vsw (kV)	C (F)	I_c (MA)	CI_c	Σ_I (S)	$-AL_{max}$(nT)	Energy (PJ)	Ionosp. energy (PJ)
9 Mar 2008	300	3,000	6.2	18,600	24	1,400	1.99	0.95
26 Feb 2008	40	8,000	2.1	16,200	9	60	0.37	0.095

3.2. The 26 February 2008 Results

The Kyoto AL index, SuperMAG SML index, and WINDMI output for the two weak events that occurred on 26 February 2008 are shown in Figure 5. The two reported substorm onsets are marked by red vertical dotted lines at min 245 (04:05 UT) and min 295 (04:55 UT). Several surges can be seen in the AL signature, but only two distinct surges are observed in the SML index. The SML index second surge occurs later than both the Kyoto AL and the WINDMI AL indices. The substorms were initiated in the model for $C = 8{,}000$ F, $\Sigma = 8.8$ S, and $I_c = 2.1$ MA. The global oscillation period here is about 70 min. The ionosphere conductivity $\Sigma_I = 9$ S. With the nominal time shift, the model triggers at about 04:00 UT, and at about 04:48 UT. If an additional shift of 5 min is added, based on onset matching, the model now triggers at 04:05 UT and 04:53 UT. This is done with the parameters held fixed. These onset times are very close to the reported values. However, the model also triggers a third time, at 04:23 UT with nominal time shift (04:28 UT with an additional 5 mins shift). This triggered event is as a result of the inherent dynamics of the WINDMI model. Because the solar wind is active throughout the hour from 04:00 to 5:00 UT, there is sufficient energy for three triggered events, as far as the model is concerned, with the optimized value of I_c.

In Figure 6, the top panel shows the model cross-tail electric field, and the bottom panel shows the model geotail current. As in the previous case, we estimate the energy budget for this event using the electric field and geotail current plots in Figure 6. The energy flow W is calculated from 03:50 UT to 05:20 UT. Here $T = 90$ min encompasses both substorms. The total energy flow over the substorm interval is 0.37 PJ according to the model. The energy transferred to the ionosphere is 0.095 PJ, or roughly one quarter of the total energy transfer, over this substorm interval.

Several surges in AL are observed between the two onsets. The reason(s) for these surges are unclear, although pseudobreakups are possible. These surges were not observed in the SML index.

4. Discussion

The disparity in solar wind driving conditions between the two intervals, 9 March 2008 and 26 February 2008, result in contrasting substorm behavior. The 9 March event occurs when the solar wind voltage was at 300-kV levels lasting over roughly 25 min prior to onset. On the other hand, the solar wind voltage was at 50-kV levels lasting over 75 min overlapping the onset times during the 26 February 2008 events.

The values produced in Table 1 were obtained by optimizing the four WINDMI model parameters against the AL/SML indices, in order to trigger a substorm at about the right time, and to generate the correct levels of peak activity. In previous work (Spencer et al., 2007), we used a genetic algorithm to optimize all the parameters of the model against both the AL and the Dst indices. This resulted in some of the optimized parameters not showing clear trends across events. Therefore, here we chose to focus our attention only the four parameters most closely related to substorm timing and AL/SML activity levels. All the others were held constant. In addition, we do not vary the time shift in the data while optimizing the parameters. Thus, the model is tightly constrained once the propagation time is fixed.

The effect of the parameters on the character and level of the produced substorm are nonlinearly related. I_c changes the level of geotail current when the unloading process begins. C, Σ, and L control the shape and duration of the resulting AL surge. However, because of the nonlinearity in the model, every effect is intertwined. Each parameter does not affect the output independently. Once a time shift due to propagation from L1 is fixed, the model parameters can only be optimized to some extent before not being able to produce a substorm at all, or having an incorrect substorm signature. As a rough guide, C is robust to 10–20% changes in value, Ic and Sigma to less than 5%, and Σ_I to about 10%.

The plasma sheet capacitance value C which is a variable parameter of the WINDMI model, is 3,000 F for the 9 March event, but 8,000 F for the 26 February events. The capacitance $C = \rho_m L_x L_z/(B^2 L_y)$ represents the inertia in the plasma sheet to changes in the $E \times B$ flows. Here ρ_m is the approximate plasma sheet

density, B is the plasma sheet average B_z, and L_x, L_y, L_z are the dimensions of the plasma sheet. The larger the value of capacitance, the slower the plasma sheet responds to changes in the solar wind electric field. Hence, the smaller electric fields during the 26 February events that lasted for a long period of time established flows comparable to those produced by the larger electric fields lasting for a short period of time that occurred during the 9 March event, that is, the maximum stored energy values $1/2CV^2$ are comparable. For the 9 March event it is $1/2\times$ 3,000 $\times(2.5)^2 \times L_y^2 = 76.3$ TJ, while for the 26 February events, it is $1/2\times$ 8,000 $\times(1)^2 \times L_y^2 = 32.6$ TJ.

The critical current I_c is also a parameter of the model. When the geotail current exceeds this critical current limit, it is assumed that current driven instabilities or other types of instabilities start to develop that initiate a substorm. The critical current is 6.2 MA on 9 March, but only 2.1 MA on 26 February. Interestingly, the capacitance values and critical current values empirically appear to have a $CI_c = k$ dependence, where k is a constant. In fact, $CI_c = 18.6 \times 10^3$ for 9 March 2008 and $CI_c = 16.2 \times 10^3$ for 26 February 2008. This apparent empirical dependence needs to be investigated across multiple substorm data sets before any firm conclusions can be drawn.

The plasma sheet conductivity, Σ, although variable, was not substantially different between the two events, $\Sigma = 8.8$ S for the 9 March 2008 event and $\Sigma = 8$ S for the 26 February 2008 event. Setting them both at 8.4 S, midway between the two values, had little impact. This had the convenient effect of further reducing the dependency of the model to just three parameters, C, I_c, and Σ_I for the two events.

The ionosphere conductivity Σ_I obtained from the model was 24 S on 9 March 2008, but only 9 S on 26 February 2008. The F10.7 solar flux index obtained from the Canadian Space Weather Forecast Centre (CSWFC) during both these events show very little difference, both days adjusted readings were between 68 and 69. The reason for the enhanced conductivity values may be due to a direct effect of the solar wind electric field via the polar caps, or from strong region 1 currents increasing the ionization rates.

The total energy budget for each substorm, as calculated with the model, can be simply understood by multiplying the rectified *VBs* voltage by the geotail current and then integrated over the event interval. Because the geotail inductance was held constant, and the time period of activity not too different ($T = 70$ for 3 March 2008 and $T = 90$ for 26 February 2008), the major contributor to the obtained energy values was the solar wind voltage.

However, the amount of energy deposited in the ionosphere as a proportion of the total energy budget is a function of several model parameters in addition to Σ_I and the level of solar wind forcing. The two substorm intervals analyzed here exhibit different characteristics. The first transfers about 50% of the total energy to the ionosphere, while the second transfers a 25%, according to the model. It is still a function of the level of solar wind activity, but the ratio of energy to ionosphere to total energy is not constant.

It should be mentioned that the additional onset triggered in the model on 26 February 2008, is as a direct result of the model parameters being optimized to produce the onsets at 4:05 UT and 4:55 UT. This is a limitation in the model that cannot be addressed unless some new modifications are made to the critical geotail current parameter I_c. For sustained levels of forcing the model will continue to produce onsets as a loading-unloading cycle repeats. This behavior was previously investigated in Spencer et al. (2007) in the case of periodic substorms repeating every 2.5 to 3 hr.

5. Conclusions

We analyzed two disparate substorm intervals with the WINDMI model. These substorm intervals were selected because we wanted to investigate whether the model behaved in a systematic and consistent way for different levels of solar wind forcing.

The model was able to capture the reported onsets, but the trigger times are dependent on the applied time shift on the solar wind input, and subject to limitations inherent in the model. Energy budgets were calculated and were within an acceptable range, following Tanskanen et al. (2002a). Furthermore, the percentage of energy deposited in the ionosphere was estimated and found to be consistent with previous authors results (Tanskanen et al., 2002b).

In order to refine the analysis, most of the model parameters were fixed, only four parameters allowed to vary. With this constraint in place, the model performed very consistently. In our previous optimization work,

using the computational Genetic Algorithm (GA) (Patra et al., 2011; Spencer et al., 2007), the parameters fluctuated inconsistently although the fitting measures were minimized. Here with manual optimization of less parameters, we have less fluctuation in the parameters, and were still able to control the model behavior. For the larger substorm, the product of plasma sheet capacitance C and critical geotail current I_c was 3000 F × 6.2 MA = 18,600, while for the smaller substorms, CI_c was 8,000 F × 2.1 MA = 16,200. This apparent inverse dependence is a new feature that needs to be thoroughly investigated in future work.

The model parameters for each type of substorm are different but are within physically acceptable bounds. There is a strong dependence of the optimized plasma sheet capacitance C and critical current parameter I_c on solar wind conditions, consistent with earlier investigations performed using the model.

A larger substorm data set needs to be studied with the WINDMI model in order to establish the interdependencies between model parameters and on the dependence on solar wind or ionosphere/magnetosphere conditions. This is left for future work.

Appendix A: WINDMI Model

The nonlinear physics-based WINDMI model uses the solar wind velocity and IMF to generate V_{sw}, a voltage coupling function, that is then used as input into eight ordinary differential equations. The differential equations represent the physics coupling the largest energy reservoirs of the nightside magnetosphere.

Further details of the WINDMI model can be found in Doxas et al. (2004), Spencer et al. (2007), and Patra et al. (2011). The plasma physics-based equations of the model are listed below:

$$L\frac{dI}{dt} = V_{sw}(t) - V + M\frac{dI_1}{dt} \tag{A1}$$

$$C\frac{dV}{dt} = I - I_1 - I_{ps} - \Sigma V \tag{A2}$$

$$\frac{3}{2}\frac{dp}{dt} = \frac{\Sigma V^2}{\Omega_{cps}} - u_0 p K_{\parallel}^{1/2}\Theta(u_1) - \frac{pVA_{eff}}{\Omega_{cps}B_{tr}L_y} - \frac{3p}{2\tau_E} \tag{A3}$$

$$\frac{dK_{\parallel}}{dt} = I_{ps}V - \frac{K_{\parallel}}{\tau_{\parallel}} \tag{A4}$$

$$L_I\frac{dI_1}{dt} = V - V_I + M\frac{dI}{dt} \tag{A5}$$

$$C_I\frac{dV_I}{dt} = I_1 - I_2 - \Sigma_I V_I \tag{A6}$$

$$L_2\frac{dI_2}{dt} = V_I - (R_{prc} + R_{A2})I_2 \tag{A7}$$

$$\frac{dW_{rc}}{dt} = R_{prc}I_2^2 + \frac{pVA_{eff}}{B_{tr}L_y} - \frac{W_{rc}}{\tau_{rc}} \tag{A8}$$

The coupled nonlinear equations of the WINDMI model describe the flow of energy through eight state variables. Several terms describe the loss of energy from the magnetosphere-ionosphere system from plasma injection, ionospheric energy deposition and ring current energy dissipation.

The coefficients of the terms in the equations are physical parameters that are estimated by averaging over regions of the magnetosphere-ionosphere system. The magnetospheric and ionospheric inductances, capacitances, and conductances are given by the parameters L, C, Σ, L_I, C_I, and Σ_I. The effective aperture for particle injection into the ring current, which merges on the dusk side with the Alfven layer (Doxas et al., 2004), is denoted as A_{eff}.

R_{prc} and R_{A2} are the resistances in the partial ring current and region 2 current I_2, respectively. The inductance of the region 2 current is L_2. In equation (A3), the coefficient u_0 is a limiting parameter for the heat flux that is generated when pressure is unloaded during a substorm. The parameters τ_E, τ_k, and τ_{rc} represent energy confinement times for the central plasma sheet, parallel kinetic energy, and ring current energy.

Table A1
Physical Parameters of the WINDMI Model, Estimated Using the Tsyganenko Geometry of the Nightside Magnetosphere

L	90 H	Inductance of the lobe cavity surrounded by the geotail current $I(t)$. The nominal value is $L = \mu_0 A_\ell / L_x^{\text{eff}}$ in Henries where A_ℓ is the lobe area and L_x^{eff} the effective length of the geotail solenoid.
M	1 H	The mutual inductance between the nightside region 1 current loop I_1 and the geotail current loop I.
C	50,000 F	Capacitance of the central plasma sheet in Farads. The nominal value is $C = \rho_m L_x L_z / (B^2 L_y)$ where ρ_m is the mass density in kg/m^3, $L_x L_z$ is the meridional area of the plasma sheet, L_y the dawn-to-dusk width of the central plasma sheet and B the magnetic field on the equatorial plane. Computations of C are given in horton 1996.
Σ	8 S	Large gyroradius ρ_i plasma sheet conductance from the quasineutral layer of height $\left(L_z \rho_i\right)^{1/2}$ about the equatorial sheet. The nominal value is $\Sigma = 0.1(n_e/B_n)(\rho_i/L_z)^{1/2}$.
Ω_{cps}	$2.6 \times 10^{24} m^3$	Volume of the central plasma sheet that supports mean pressure $p(t)$, initial estimate is $10^4 R_E^3$.
u_0	4e–9 $\text{m}^{-1}\, kg^{-1/2}$	Heat flux limit parameter for parallel thermal flux on open magnetic field lines $q_\parallel = const \times v_\parallel p = u_0 (K_\parallel)^{1/2} p$. The mean parallel flow velocity is $(K_\parallel / (\rho_m \Omega_{\text{cps}}))^{1/2}$.
I_c	1.78×10^7 A	The critical current above which unloading occurs.
α	8×10^{11}	The geotail current driven by the plasma pressure p confined in the central plasma sheet. Pressure balance between the lobe and the central plasma sheet gives $B_\ell^2 / 2\mu_0 = p$ with $2 L_x B_\ell = \mu_0 I_{\text{ps}}$. This defines the coefficient α in $I_{ps} = \alpha p^{1/2}$ to be approximately $\alpha = 2.8 L_x / \mu_0^{1/2}$.

Note. Table A2 contains the remaining parameters.

Table A2
Physical Parameters of the WINDMI Model, Estimated Using the Tsyganenko Geometry of the Nightside Magnetosphere

$\tau_\parallel$	10 min	Confinement time for the parallel flow kinetic energy $K_\parallel$ in the central plasma sheet.
τ_E	30 min	Characteristic time of thermal energy loss through earthward and tailward boundary of plasma sheet.
L_1	20 H	The self-inductance of the wedge current or the nightside region 1 current loop $I_1(t)$
C_I	800 F	The capacitance of the nightside region1 plasma current loop.
Σ_I	3 mho	The ionospheric Pedersen conductance of the westward electrojet current closing the I_1 current loop in the auroral (altitude ~100 km, 68°) zone ionosphere.
R_{prc}	0.1 ohm	The resistance of the partial ring current.
τ_{rc}	12 hr	The decay time for the ring current energy.
L_2	8 H	The inductance of the region 2 current.
R_{A2}	0.3 ohm	Resistance of the region 2 footprint in the Auroral Region.
B_{tr}	5×10^{-9} T	The magnetic field in the transition region.
A_{eff}	$8.14 \times 10^{13} m^2$	The average effective area presented to the geotail plasma for plasma entry into the inner magnetosphere, estimated to be $2R_E^2$.
L_y	3.2×10^7 m	The effective width of the Alfven layer aperture, estimated to be 5 R_E.
ΔI	1.25×10^5 A	The rate of turn-on of the unloading function.

Note. See Table A1 for the other parameters.

The magnetosphere is assumed to have an effective width given by L_y. The magnetic field in the transition region between a dipolar field and a stretched tail field is given by B_{tr}.

The current $I_{ps} = L_x(p/\mu_0)^{1/2}$, is the pressure gradient driven part of the cross-tail current, where L_x is the effective length of the magnetotail. The pressure unloading function $\Theta(u_1) = \frac{1}{2}[1 + \tanh u_1]$ where $u_1 = (I - I_c)/\Delta I$ in equation (A3).

Equation (A3) contains a critical current term I_c and the interval ΔI which indicates the loss of plasma along newly opened magnetic field lines with a parallel thermal flux $q_{||}$. It changes from zero to one as a function of $I - I_c$, following a hyperbolic tangent function. The unloading function is assumed to follow from current gradient driven tearing modes or cross-field current instabilities, as described in Yoon et al. (2002). The parameters are described briefly and estimated using some knowledge of the Earth's magnetospheric field structure in Tables A1 and A2.

The WINDMI model outputs are the AL and *Dst* indices, which are proportional to the the magnetospheric currents. The AL index is obtained from the region 1 current I_1 index by assuming a constant of proportionality λ_{AL}(A/nT), giving $\Delta B_{AL} = -I_1/\lambda_{AL}$.

The input coupling function used for the model is a rectified vB_s expression (Reiff & Luhmann, 1986):

$$V_{sw}^{Bs} = 40 \quad (\text{kV}) + v_{sw} B_s^{IMF} L_y^{eff} \quad (\text{kV}) \tag{A9}$$

where v_{sw} is the x-directed component of the solar wind velocity in GSM coordinates, B_s^{IMF} is the southward IMF component and L_y^{eff} is an effective cross-tail width over which the coupling voltage is produced. For northward or zero B_s^{IMF}, a base viscous voltage of 4 kV is assumed.

Acknowledgments
This work is partially supported by NSF EPSCOR grant 1655280. The solar wind plasma and magnetic field data were obtained from NASA CDF SPDF website from the ACE satellite measurements (http://cdaweb.gsfc.nasa.gov). The geomagnetic indices used were obtained from the World Data Center for Geomagnetism, Kyoto, Japan. The SML indices were obtained from SUPERMAG website (http://supermag.jhuapl.edu). The *E* field and *B* field data were observed in THEMIS Berkeley website and obtained from NASA CDAWeb from THEMIS B, THEMIS D, and THEMIS E satellites (http://cdaweb.gsfc.nasa.gov). The F10.7 flux values were obtained from the Canadian Space Weather Forecast Centre (CSWFC; http://www.spaceweather.gc.ca/index-en.php). The WINDMI model is available for runs upon request at the NASA Community Coordinated Modeling Center (NASA CCMC; https://ccmc.gsfc.nasa.gov/). Model parameters are at default values, except as noted here in this work.

References

Akasofu, S. I. (1981). Energy coupling between the solar wind and the magnetosphere. *Space Science Reviews*, *28*(2), 121–190. https://doi.org/10.1007/BF00218810

Akasofu, S. I. (2013). Where is the magnetic energy for the expansion phase of auroral substorms accumulated? *Journal of Geophysical Research: Space Physics*, *118*, 7219–7225. https://doi.org/10.1002/2013JA019042

Baker, D. N., Fritz, T. A., McPherron, R. L., Fairfield, D. H., Kamide, Y., & Baumjohann, W. (1985). Magnetotail energy storage and release during the CDAW 6 substorm analysis intervals. *Journal of Geophysical Research*, *90*, 1205–1216. https://doi.org/10.1029/JA090iA02p01205

Baker, D., Pulkkinen, T., Buchner, J., & Klimas, A. (1999). Substorms: A global instability of the magnetosphere-ionosphere system. *Journal of Geophysical Research*, *104*(A7), 14,601–14,611.

Doxas, I., Horton, W., Lin, W., Seibert, S., & Mithaiwala, M. (2004). A dynamical model for the coupled inner magnetosphere and tail. *IEEE Transactions on Plasma Science*, *32*(4), 1443–1448.

Forsyth, C., Rae, I. J., Coxon, J. C., Freeman, M. P., Jackman, C. M., Gjerloev, J., & Fazakerley, A. N. (2015). A new technique for determining substorm onsets and phases from indices of the electrojet (SOPHIE). *Journal of Geophysical Research: Space Physics*, *120*, 10,592–10,606. https://doi.org/10.1002/2015JA021343

Horton, W., & Doxas, I. (1996). A low-dimensional energy-conserving state space model for substorm dynamics. *Journal of Geophysical Research*, *101*(A12), 27,223–27,237.

Horton, W., & Doxas, I. (1998). A low-dimensional dynamical model for the solar wind driven geotail-ionosphere system. *Journal of Geophysical Research*, *103*(A3), 4561–4572.

Huang, C. S., & Cai, X. (2009). Magnetotail total pressure and lobe magnetic field at onsets of sawtooth events and their relation to the solar wind. *Journal of Geophysical Research*, *114*, A04204. https://doi.org/10.1029/2008JA013807

Kallio, E. I., Pulkkinen, T. I., Koskinen, H. E. J., Viljanen, A., Slavin, J. A., & Ogilvie, K. (2000). Loading-unloading processes in the nightside ionosphere. *Geophysical Research Letters*, *27*(11), 1627–1630. https://doi.org/10.1029/1999GL003694

Kullen, A., Karlsson, T., Cumnock, J. A., & Sundberg, T. (2010). Occurrence and properties of substorms associated with pseudobreakups. *Journal of Geophysical Research*, *115*, A12310. https://doi.org/10.1029/2010JA015866

Lui, A. T. Y. (2011). Revisiting time history of events and macroscale interactions during substorms (THEMIS) substorm events implying magnetic reconnection as the substorm trigger. *Journal of Geophysical Research*, *116*, A03211. https://doi.org/10.1029/2010JA016078

Mailyan, B., Munteanu, C., & Haaland, S. (2008). What is the best method to calculate the solar wind propagation delay? *Annales Geophysicae*, *26*, 2383–2394. https://doi.org/10.5194/angeo-26-2383-2008

McPherron, R. L. (1970). Growth phase of magnetospheric substorms. *Journal of Geophysical Research*, *75*(28), 5592–5599.

Meurant, M., GéRard, J.-C., Blockx, C., Spanswick, E., Donovan, E. F., Coumans, B. H. V., & Connors, M. (2007). El—A possible indicator to monitor the magnetic field stretching at global scale during substorm expansive phase: Statistical study. *Journal of Geophysical Research*, *112*, A05222. https://doi.org/10.1029/2006JA012126

Miyashita, Y., Kamide, Y., Machida, S., Liou, K., Mukai, T., Saito, Y., et al. (2004). Difference in magnetotail variations between intense and weak substorms. *Journal of Geophysical Research*, *109*, A11205. https://doi.org/10.1029/2004JA010588

Nakai, H., & Kamide, Y. (2005). Time constants of Earth's magnetotail for responding to a southward excursion of IMF: The super high pressure magnetotail event of 10 December 1996. *Journal of Geophysical Research*, *110*, A09225. https://doi.org/10.1029/2004JA010957

Newell, P. T., & Gjerloev, J. W. (2011a). Evaluation of SuperMAG auroral electrojet indices as indicators of substorms and auroral power. *Journal of Geophysical Research*, *116*, A12211. https://doi.org/10.1029/2011JA016779

Newell, P. T., & Gjerloev, J. W. (2011b). Substorm and magnetosphere characteristic scales inferred from the SuperMAG auroral electrojet indices. *Journal of Geophysical Research*, *116*, A12232. https://doi.org/10.1029/2011JA016936

Newell, P., Sorelis, T., Liou, K., Meng, C.-I., & Rich, F. (2007). A nearly universal solar wind-magnetosphere coupling function inferred from 10 magnetospheric state variables. *Journal of Geophysical Research*, *112*, A01206. https://doi.org/10.1029/2006JA012015

Ohtani, S., & Uozumi, T. (2014). Nightside magnetospheric current circuit: Time constants of the solar wind-magnetosphere coupling. *Journal of Geophysical Research: Space Physics*, *119*, 3558–3572. https://doi.org/10.1002/2013JA019680

Partamies, N., Juusola, L., Tanskanen, E., & Kauristie, K. (2013). Statistical properties of substorms during different storm and solar cycle phases. *Annales Geophysicae*, *31*(2), 349–358. https://doi.org/10.5194/angeo-31-349-2013

Patra, S., Spencer, E., Horton, W., & Sojka, J. (2011). Study of Dst/ring current recovery times using the WINDMI model. *Journal of Geophysical Research*, *116*, A02212. https://doi.org/10.1029/2010JA015824

Pu, Z. Y., Chu, X. N., Caoa, X., Mishin, V., Angelopoulos, V., Wang, J., et al. (2010). THEMIS observations of substorms on 26 February 2008 initiated by magnetotail reconnection. *Journal of Geophysical Research*, *115*, A02212. https://doi.org/10.1029/2009JA014217

Reiff, P. H., & Luhmann, J. G. (1986). Solar wind control of the polar-cap voltage. In Y. Kamide & J. A. Slavin (Eds.), *Solar Wind-Magnetosphere Coupling* (pp. 453–476). Tokyo: Terra Science.

Spencer, E., Horton, W., Mays, L., Doxas, I., & Kozyra, J. (2007). Analysis of the 3–7 October 2000 and 15–24 April 2002 geomagnetic storms with an optimized nonlinear dynamical model. *Journal of Geophysical Research*, *112*, A04S90. https://doi.org/10.1029/2006JA012019

Spencer, E., Kasturi, P., Patra, S., Horton, W., & Mays, M. L. (2011). Influence of solar wind magnetosphere coupling functions on the Dst index. *Journal of Geophysical Research*, *116*, A12235. https://doi.org/10.1029/2011JA016780

Spencer, E., Rao, A., Horton, W., & Mays, M. L. (2009). Evaluation of solar wind-magnetosphere coupling functions during geomagnetic storms with the WINDMI model. *Journal of Geophysical Research*, *114*, A02206. https://doi.org/10.1029/2008JA013530

Tanskanen, E., Koskinen, H., Pulkkinen, T., Slavin, J., & Ogilvie, K. (2002b). Dissipation to the Joule heating: Isolated and stormtime substorms. *Journal of Advances in Space Research*, *30*, 2305–2311. https://doi.org/10.1016/S0273-1177(02)80254-X

Tanskanen, E., Pulkkinen, T. I., & Koskinen, H. E. J. (2002a). Substorm energy budget during low and high solar activity: 1997 and 1999 compared. *Journal of Geophysical Research*, *107*(A6), 1086. https://doi.org/10.1029/2001JA900153

Weimer, D. R., & King, J. H. (2008). Improved calculations of IMF phase front angles and propagation time delays. *Journal of Geophysical Research*, *113*, A01105. https://doi.org/10.1029/2007JA012452

Xing, X., Lyons, L., Nishimura, Y., Angelopoulos, V., Larson, D., Carlson, C., et al. (2010). Substorm onset by new plasma intrusion: THEMIS spacecraft observations. *Journal of Geophysical Research*, *115*, A10246. https://doi.org/10.1029/2010JA015528

Yoon, P., Lui, A., & Sitnov, M. (2002). Generalized lower-hybrid drift instabilities in current sheet equilibrium. *Physics of Plasmas*, *9*(5), 1526–1538.